

Double-scattering mechanism in exclusive $AA \rightarrow AA\rho^0\rho^0$ reaction at ultrarelativistic collisions

Mariola Klusek-Gawenda*

Institute of Nuclear Physics PAN, PL-31-342 Cracow, Poland

Antoni Szczurek†

*Institute of Nuclear Physics PAN, PL-31-342 Cracow, Poland and
University of Rzeszów, PL-35-959 Rzeszów, Poland*

(Dated: February 26, 2022)

Abstract

We calculate, for the first time, differential distributions for double ρ^0 meson production in exclusive ultraperipheral, ultrarelativistic collisions via a double scattering mechanism. The calculations are done in impact parameter space. The cross section for $\gamma A \rightarrow \rho^0 A$ is parametrized based on an existing calculation. Smearing of ρ^0 masses is taken into account. The results of our calculations are compared at the RHIC energy to the contribution of the two-photon mechanism discussed previously in the literature. The cross section for the double scattering mechanism is found to be an order of magnitude larger at $M_{\rho\rho} < 2$ GeV and more than two orders of magnitude at $M_{\rho\rho} > 3$ GeV, than that for the photon-photon mechanism. Compared to the two-photon mechanism the double scattering mechanism populates somewhat larger $\rho^0\rho^0$ invariant masses and larger rapidity distances between the two ρ^0 mesons and gives a significant contribution to the $AA \rightarrow AA\pi^+\pi^-\pi^+\pi^-$ reaction. Some observables related to charged pions are presented too. We compare the results of our calculation with the STAR collaboration results on four charged pion production. While the shape in invariant mass of the four-pion system is very similar to the measured one, the predicted cross section constitutes only 20 % of the measured one. We discuss a possibility of identifying the double scattering mechanism at the LHC.

PACS numbers: 25.75.Dw -Particle production (relativistic collisions)
13.25.-k -Decay mesons hadronic

*Electronic address: mariola.klusek@ifj.edu.pl

†Electronic address: antoni.szczurek@ifj.edu.pl

I. INTRODUCTION

The exclusive production of simple final states in ultraperipheral, ultrarelativistic heavy ion collisions is a special class of nuclear reactions [1]. At high energies and due to large charges of colliding nuclei there are two categories of the underlying reaction mechanisms. One is the photon-photon fusion and the second is photoproduction (photon fluctuation into hadronic or quark-antiquark components and its transformation into a simple final state). The competition between these two mechanisms was studied only for few cases.

For $\rho^0\rho^0$ production only the photon-photon mechanism was discussed in the literature [2–4]. In Ref. [2] we have made a first realistic estimate of the corresponding cross section.

The cross section for single meson production was predicted to be large [5–7]. Measurements at RHIC confirmed the size of the cross section [8] at midrapidities, but were not able to distinguish between different models that predicted different behaviour at large (unmeasured) (pseudo)rapidities. The large cross section for single ρ^0 production suggests that the cross section for double scattering process should be also rather large. The best example of a similar type of reaction is the production of $c\bar{c}c\bar{c}$ final state in proton-proton collisions which was measured recently by the LHCb collaboration [9]. This was predicted and explained in Ref. [10] as a double-parton scattering effect. There, the cross section for the $c\bar{c}c\bar{c}$ final state is of the same order of magnitude as the cross section for single $c\bar{c}$ pair production. The situation for exclusive ρ^0 production is somewhat similar. Due to easier control of absorption effect, the impact parameter formulation seems in the latter case the best approach.

In the present paper, we wish to focuss on double ρ^0 production in ultraperipheral, ultrarelativistic heavy ion reactions. We wish to study differential single particle distributions for the ρ^0 mesons, as well as correlations between the ρ mesons, also for the photon-photon component. A comparison to the results for photon-photon process will be done too, in order to understand how to identify the double photoproduction process. We intend to take into account the decay of ρ^0 mesons into charged pions, in order to take into account some experimental cuts of existing experiments. We shall discuss how to identify the double-scattering mechanism at the LHC.

II. FORMALISM

A. Single scattering mechanisms

Most of the previous analyses in the literature concentrated on production of pairs of mesons in photon-photon processes (see Fig. 1). In the past we have studied both exclusive $\rho^0\rho^0$ productions [2] and recently exclusive production of $J/\psi J/\psi$ pairs.

In the case of double ρ^0 production there are two mechanisms. At larger photon-photon energies the pomeron/reggeon exchange mechanism is the dominant one, while close to $\rho^0\rho^0$ threshold a large enhancement was observed. The latter mechanism is not well understood. In Ref. [2] this enhancement of the cross section was parametrized. In the present paper we shall concentrate rather on larger photon-photon energies (larger dimeson invariant masses).

In the case of double J/ψ production there are also two distinct mechanisms. At low photon-photon energies a box mechanism dominates, and at larger energies the two-gluon exchange mechanism takes over.

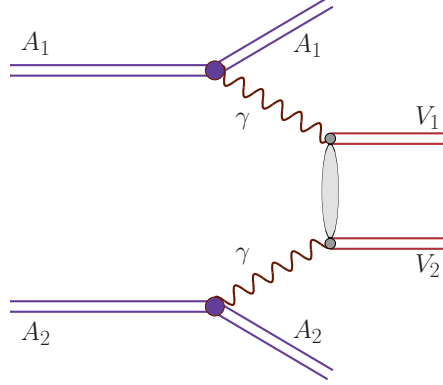


FIG. 1: The photon-photon mechanism of two vector meson production in ultrarelativistic ultra-peripheral collisions.

The elementary cross section for $\gamma\gamma \rightarrow \rho^0\rho^0$ has been measured in the past [11] for not too large energies. The measured cross section shows a characteristic bump at about $M_{\rho\rho} \sim 1.5$ GeV. The origin of this bump is so far not well understood. In Ref. [2] we have parametrized the measured cross section and used the resulting elementary cross section as the input for nuclear calculations.

There are many potential mechanisms contributing to the bump. Since the calculation of the corresponding cross sections is not always easy, we leave theoretical studies of the underlying dynamics for future studies. At somewhat larger photon-photon energies ($\rho^0\rho^0$ invariant masses in the case of nuclear collisions) another mechanism, which can be relatively well calculated, plays the dominant role, namely soft virtual (quasi-real) vector meson rescattering. The corresponding matrix element for not too large ρ^0 meson transverse momenta can be parametrized in the VDM-Regge language [2]. At large transverse momenta of the ρ^0 meson, two-gluon exchange should become important (see a discussion of two-gluon exchange for $J/\Psi J/\Psi$ production in Ref. [12]). In the present analysis we shall discuss only the soft scattering mechanisms. The hard mechanism may be important at the LHC. It is interesting if the two mechanisms can be identified by imposing kinematical cuts, or by looking at special observables.

The nuclear cross section for the photon-photon mechanism is calculated in the impact parameter space as:

$$\sigma(AA \rightarrow AA\rho^0\rho^0) = \int \hat{\sigma}(\gamma\gamma \rightarrow \rho^0\rho^0; W_{\gamma\gamma}) S_{abs}^2(\mathbf{b}) N(\omega_1, \mathbf{b}_1) N(\omega_2, \mathbf{b}_2) \times d^2\mathbf{b}_1 d^2\mathbf{b}_2 d\omega_1 d\omega_2, \quad (2.1)$$

where

$$S_{abs}^2(\mathbf{b}) = \theta(\mathbf{b} - 2R_A) = \theta(|\mathbf{b}_1 - \mathbf{b}_2| - 2R_A). \quad (2.2)$$

This can be written equivalently as:

$$\sigma(AA \rightarrow AA\rho^0\rho^0) = \int \hat{\sigma}(\gamma\gamma \rightarrow \rho^0\rho^0; W_{\gamma\gamma}) S_{abs}^2(\mathbf{b}) N(\omega_1, \mathbf{b}_1) N(\omega_2, \mathbf{b}_2) \times \frac{W_{\gamma\gamma}}{2} d^2\mathbf{b}_1 d^2\mathbf{b}_2 dW_{\gamma\gamma} dY_{\rho^0\rho^0}. \quad (2.3)$$

Four-momenta of ρ^0 mesons in the $\rho^0\rho^0$ center of mass frame can be written as:

$$E_{\rho^0} = \frac{\sqrt{\hat{s}}}{2} , \quad (2.4)$$

$$p_{\rho^0} = \sqrt{\frac{\hat{s}}{4} - m_{\rho^0}^2} , \quad (2.5)$$

$$p_{t,\rho^0} = \sqrt{1 - z^2} p_{\rho^0} , \quad (2.6)$$

$$p_{l,\rho^0} = z p_{\rho^0} . \quad (2.7)$$

The rapidity of each of the ρ^0 mesons ($i = 1, 2$) can be calculated as:

$$y_i = Y_{\rho^0\rho^0} + y_{i/\rho^0\rho^0}(W, z) , \quad (2.8)$$

where z is related to ρ^0 meson transverse momentum. Other kinematical variables are calculated by adding relativistically velocities:

$$\vec{v}_i = \vec{V}_{\rho^0\rho^0} \oplus \vec{v}_{i/\rho^0\rho^0} , \quad (2.9)$$

$$\vec{V}_{\rho^0\rho^0} = \frac{\vec{P}_{\rho^0\rho^0}}{E_{\rho^0\rho^0}} . \quad (2.10)$$

The energies of photons can be expressed in terms of our integration variables

$$\omega_{1/2} = \frac{W_{\gamma\gamma}}{2} \exp(\pm Y_{\rho^0\rho^0}) \quad (2.11)$$

from the energy-momentum conservation:

$$\begin{aligned} E_{\rho^0\rho^0} &= \omega_1 + \omega_2 , \\ P_{\rho^0\rho^0}^z &= \omega_1 - \omega_2 . \end{aligned} \quad (2.12)$$

The total elementary cross section can be calculated as:

$$\hat{\sigma}(\gamma\gamma \rightarrow \rho^0\rho^0) = \int_{t_{min}(\hat{s})}^{t_{max}(\hat{s})} \frac{d\hat{\sigma}}{d\hat{t}} d\hat{t} , \quad (2.13)$$

where

$$\frac{d\hat{\sigma}(\gamma\gamma \rightarrow \rho^0\rho^0)}{d\hat{t}} = \frac{1}{16\pi\hat{s}^2} |\mathcal{M}_{\gamma\gamma \rightarrow \rho^0\rho^0}|^2 . \quad (2.14)$$

The high $W_{\gamma\gamma}$ -(sub)energy matrix element is calculated in a VDM-Regge approach [2] as

$$\begin{aligned} \mathcal{M}_{\gamma\gamma \rightarrow \rho^0\rho^0} &= C_{\gamma \rightarrow \rho^0} C_{\gamma \rightarrow \rho^0} \hat{s} \left(\eta_{\mathbf{P}}(\hat{s}, \hat{t}) C_{\mathbf{P}} \left(\frac{\hat{s}}{s_0} \right)^{\alpha_{\mathbf{P}}(t)-1} + \eta_R(\hat{s}, \hat{t}) C_R \left(\frac{\hat{s}}{s_0} \right)^{\alpha_R(t)-1} \right) \\ &\times F(\hat{t}, q_1^2 \approx 0) F(\hat{t}, q_2^2 \approx 0) . \end{aligned} \quad (2.15)$$

This seems to be consistent with the existing world experimental data on total $\gamma\gamma \rightarrow \rho^0\rho^0$ cross section [2]. The $C_{\gamma \rightarrow \rho^0}$ factors, describing transformation of photons to (virtual) vector mesons, are calculated in the Vector Dominance Model (VDM). The parameters responsible

for energy dependence are taken from the Donnachie-Landshoff parametrization of the total proton-proton and pion-proton cross sections [13] assuming Regge factorization. The slope parameter (B) is taken to be $B = 4 \text{ GeV}^{-2}$. How the form factors $F(\hat{t}, q^2)$ are parametrized is described in detail in Ref. [2]. When calculating kinematical variables, a fixed resonance position $m_\rho = m_R$ is taken for the $\gamma\gamma \rightarrow \rho^0\rho^0$. Mass smearing could be included if necessary.

The differential distributions can be obtained by replacing total elementary cross section by

$$\hat{\sigma}(\gamma\gamma \rightarrow \rho^0\rho^0) = \int \frac{d\hat{\sigma}(\gamma\gamma \rightarrow \rho^0\rho^0)}{dp_t} dp_t, \quad (2.16)$$

where

$$\frac{d\hat{\sigma}}{dp_t} = \frac{d\hat{\sigma}}{dp_t^2} \frac{dp_t^2}{dp_t} = \frac{d\hat{\sigma}}{dp_t^2} 2p_t = \frac{d\hat{\sigma}}{d\hat{t}} |\partial\hat{t}/\partial p_t^2| 2p_t. \quad (2.17)$$

The first ρ^0 is emitted in the forward and the second ρ^0 in the backward direction in the $\gamma\gamma \rightarrow \rho^0\rho^0$ center-of-mass system. Finally the following three-dimensional maps (grids) are prepared separately for the low-energy bump and VDM-Regge components:

$$\frac{d\sigma_{AA \rightarrow AA\rho^0\rho^0}}{dy_1 dy_2 dp_t}. \quad (2.18)$$

The maps (grids) are used then to calculate distributions of pions from the decays of ρ^0 mesons produced in the photon-photon fusion.

B. Single ρ^0 production

The cross section for single vector meson production, differential in impact factor and vector-meson rapidity, reads:

$$\frac{d\sigma}{d^2b dy} = \omega_1 \frac{d\tilde{N}}{d^2b d\omega_1} \sigma_{\gamma A_2 \rightarrow V A_2}(W_{\gamma A_2}) + \omega_2 \frac{d\tilde{N}}{d^2b d\omega_2} \sigma_{\gamma A_1 \rightarrow V A_1}(W_{\gamma A_1}), \quad (2.19)$$

where $\omega_1 = m_{\rho^0}/2 \exp(+y)$ and $\omega_2 = m_{\rho^0}/2 \exp(-y)$. Here the flux factor of equivalent photons, \tilde{N} , is in principle a function of heavy ion - heavy ion impact parameter b and not of photon-nucleus impact parameter as is often done in the literature. The effective impact factor can be formally written as the convolution of real photon flux in one of the nuclei and effective strength for interaction of the photon with the second nucleus

$$\frac{d\tilde{N}}{d^2b d\omega} = \int \frac{dN}{d^2b_1 d\omega} \frac{S(b_2)}{\pi R_A^2} d^2b_1 \approx \frac{dN}{d^2b d\omega}, \quad (2.20)$$

where $\vec{b}_1 = \vec{b} + \vec{b}_2$ and $S(b_2) = \theta(R_A - b_2)$, i.e., it is assumed that the collision occurs when the photon hits the nucleus. For the photon flux in the second nucleus one needs to replace $1 \rightarrow 2$ (and $2 \rightarrow 1$).

In general one can write:

$$\sigma_{\gamma A \rightarrow V A}(W) = \frac{d\sigma_{\gamma A \rightarrow V A}(W, t=0)}{dt} \int_{-\infty}^{t_{max}} dt |F_A(t)|^2. \quad (2.21)$$

The second factor includes the t -dependence for the $\gamma A \rightarrow VA$ subprocess which is due to coherent $q\bar{q}$ dipole rescattering off a nucleus. To good approximation this is dictated by the nuclear strong form factor. In practical calculations, we approximate the nuclear strong form factor by the nuclear charge form factor. The t_{max} is calculated from kinematical dependences, $t_{max} = -(m_{\rho^0}^2/(2\omega_{lab}))^2$. The first term in Eq. (2.21) is usually weakly dependent on the γA energy. For the ρ^0 meson it is practically a constant [5]:

$$\frac{d\sigma(\gamma + A \rightarrow \rho^0 A; t = 0)}{dt} \approx \text{const} . \quad (2.22)$$

In the present exploratory calculation the constant is taken to be (see [5]) 420 mb/GeV² for RHIC and 450 mb/GeV² for LHC. These are cross sections for $W_{\gamma p}$ energies relevant for midrapidities at $\sqrt{s_{NN}} = 200$ GeV and 5.5 TeV, respectively.

A more refined treatment will be presented elsewhere when discussing different models of ρ^0 photoproduction. The second term depends on t_{max} which in turn depends rather on running ρ^0 meson mass than on resonance position.

The cross section for the $\gamma A \rightarrow VA$ reaction could be also calculated e.g., in the QCD dipole picture in a (convenient) so-called mixed representation (see e.g., [14, 15]). Slightly more complicated momentum space formulation of the vector meson production on nuclei was discussed in Ref. [16].

At high energy the imaginary part of the amplitude for the $\gamma A \rightarrow VA$ process can be written as [17, 18]:

$$\Im(A_{\gamma A \rightarrow VA}(W)) = \Sigma_{\lambda\bar{\lambda}} \int dz d^2\rho \Psi_{\lambda\bar{\lambda}}^V(z, \rho) \sigma_{dip-A}(W, \rho) \Psi_{\lambda\bar{\lambda}}^\gamma(z, \rho)(z, \rho) . \quad (2.23)$$

In the equation above, λ and $\bar{\lambda}$ are quark and antiquark helicities. Helicity conservation at high energy rescattering of the dipole in the nucleus is explicitly assumed. The variable ρ is the transverse size of the quark-antiquark dipole, and z denotes the longitudinal momentum fraction carried by quark. The longitudinal momentum fraction carried by antiquark is then $(1 - z)$. Using explicit formulae for photon and vector meson wave functions, the generic formula (2.23) can be written in a convenient way (for calculation see [14]). The dipole-nucleus cross section can then be expressed in the Glauber-Gribov picture in terms of the nuclear thickness $T_A(b_\gamma)$, as seen by the $q\bar{q}$ dipole in its way through the nucleus, and the dipole-proton $\sigma_{dip-p}(\rho)$ cross section as (see e.g., [19]):

$$\sigma_{dip-A}(\rho, W) = 2 \int d^2b_\gamma \left\{ 1 - \exp \left(-\frac{1}{2} T_A(b_\gamma) \sigma_{dip-p}(\rho, W) \right) \right\} . \quad (2.24)$$

This simple formula allows for an easy and convenient way to include rather complex multiple scattering of the quark-antiquark dipole in the nucleus. Several parametrizations of the dipole-nucleon cross section have been proposed in the literature. Most of them were obtained through fitting HERA deep-inelastic scattering data which, in principle, does not allow for unique extraction of the functional form. The saturation inspired parametrizations are the most popular and topical at present.

Before we go to double ρ^0 production, we shall briefly show as an example the results for single ρ^0 production. In Fig. 2 we present distributions in rapidity. We obtain similar results as in other calculations in the literature [5–7]. Given the approximate character of the model (see also Eq. (2.22)) the agreement is rather satisfactory. Our total cross section equals 596 mb, compared to 590 mb in the original Klein-Nystrand model [5]. The results of models presented in [6] and [7] exceed the STAR experimental data [8].

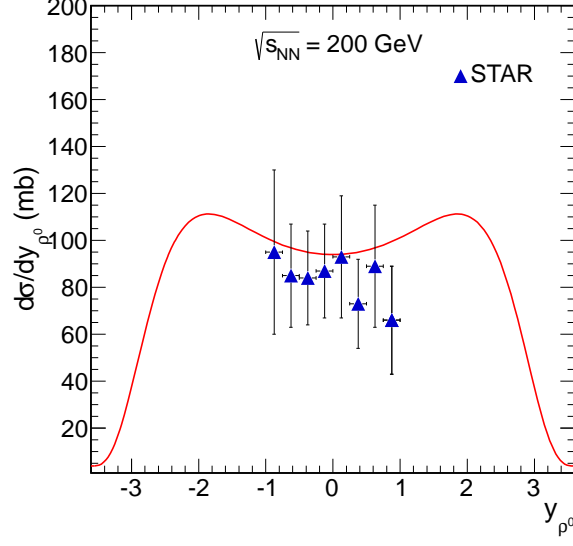


FIG. 2: Distribution in ρ^0 rapidity for single ρ^0 production. The STAR experimental data are taken from Ref. [8].

C. Double scattering mechanism

The generic diagrams of double-scattering production via photon-pomeron or pomeron-photon exchange ¹ mechanism are shown in Fig. 3.

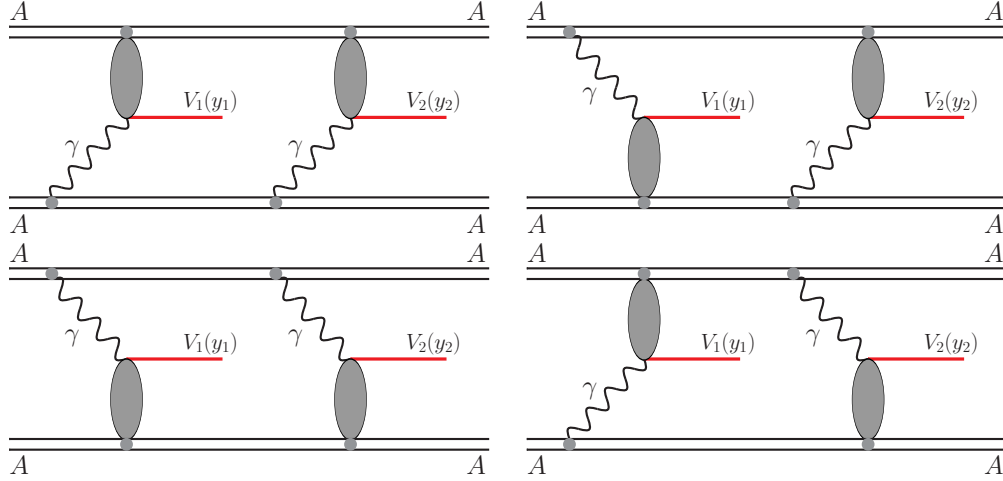


FIG. 3: The double-scattering mechanisms of two vector meson production in ultrarelativistic, ultraperipheral collisions. The blobs denote multiple scattering of quark-antiquark dipoles or hadronic meson-like photon in the nucleus termed here “pomeron exchange” for brevity.

The double scattering process was discussed only in Ref. [5], where only a probabilistic

¹ By “pomeron exchange” we mean here rather high-energy multiple diffractive rescattering of quark-antiquark pairs (see e.g., [16]) or virtual vector mesons.

formula for double and multiple vector meson production was given. For example the cross section for double scattering can be written as:

$$\sigma_{AA \rightarrow AAV_1 V_2}(\sqrt{s_{NN}}) = C \int S_{el}^2(b) P_{V_1}(b, \sqrt{s_{NN}}) P_{V_2}(b, \sqrt{s_{NN}}) d^2b . \quad (2.25)$$

In the equation above b is the impact parameter (transverse distance between nuclei). We have included natural limitations in the impact parameter

$$S_{el}^2(b) = \exp(-\sigma_{NN}^{tot} T_{A_1 A_2}(b)) \approx \theta(b - (R_1 + R_2)) . \quad (2.26)$$

It may be interpreted as a survival probability for nuclei not to break up. The probability density of single meson production is

$$P_V(b, \sqrt{s_{NN}}) = \frac{d\sigma_{AA \rightarrow AAV}(b; \sqrt{s_{NN}})}{2\pi b db} . \quad (2.27)$$

The constant C is in the most general case 1 or $\frac{1}{2}$ for identical vector mesons $V_1 = V_2$. We have explicitly indicated the dependence of the probabilities on nucleon-nucleon energy. The probability densities P_V increase with increasing cm energy.

The photon flux factor is calculated here as:

$$\frac{d^3 N}{d^2 b d\omega} = \frac{Z^2 \alpha_{em} X^2}{\pi^2 \omega b^2} K_1^2(X) , \quad (2.28)$$

where $X = \frac{b\omega}{\gamma}$. We leave a more refined treatment for future studies.

The simple formula (2.25) can be generalized to calculate two-dimensional distributions in rapidities of both vector mesons

$$\begin{aligned} \frac{d\sigma_{AA \rightarrow AAV_1 V_2}}{dy_1 dy_2} = C \int & \left(\frac{dP_1^{\gamma \mathbf{IP}}(b, y_1; \sqrt{s_{NN}})}{dy_1} + \frac{dP_1^{\mathbf{IP} \gamma}(b, y_1; \sqrt{s_{NN}})}{dy_1} \right) \\ & \times \left(\frac{dP_2^{\gamma \mathbf{IP}}(b, y_2; \sqrt{s_{NN}})}{dy_2} + \frac{dP_2^{\mathbf{IP} \gamma}(b, y_2; \sqrt{s_{NN}})}{dy_2} \right) d^2b . \end{aligned} \quad (2.29)$$

P_1 and P_2 are probability densities for producing one vector meson V_1 at rapidity y_1 and the second vector meson V_2 at rapidity y_2 for fixed impact parameter b of the heavy-ion collision. Then the differential probability density can be written as:

$$\frac{dP_V(b, \sqrt{s_{NN}})}{dy} = \frac{d\sigma_{AA \rightarrow AAV}(b; \sqrt{s_{NN}})}{2\pi b db dy} . \quad (2.30)$$

The produced vector mesons in each step are produced in very broad range of (pseudo)rapidity [5, 14] and extremely small transverse momenta.

D. Smearing the ρ^0 masses

The ρ^0 resonance is fairly broad. We consider two different approximations: (a) fixed ρ^0 mass, (b) smeared mass. In the fixed-mass approximation, the mass of the di-meson system (for identical vector meson masses) can be calculated from the simple formula

$$M_{\rho^0 \rho^0}^2 = 2m_{\rho^0}^2 (1 + \cosh(y_1 - y_2)) . \quad (2.31)$$

The mass is then calculated for each phase space point (y_1, y_2) (see Eq. (2.29)) and put into a histogram.

In a more refined approximation (b) one has to include in addition a smearing of the ρ^0 mass. Then the cross section can be written as:

$$\frac{d\sigma_{AA \rightarrow AA\rho_0^*\rho_0^*}}{dm_1 dm_2 dy_1 dy_2} = f(m_1)f(m_2) \frac{d\sigma_{AA \rightarrow AA\rho_0^*\rho_0^*}}{dy_1 dy_2}(y_1 y_2; m_1, m_2) , \quad (2.32)$$

where m_1 and m_2 are the running masses of ρ^0 mesons and $f_1(m_1)$ and $f_2(m_2)$ are smearing distributions spectral shapes as used below. The last term is the production cross section for running ρ^0 meson masses m_1 and m_2 . In general, the cross section depends on the values of the ρ^0 masses. The smaller the mass, the larger the cross section. In the present analysis the spectral shapes are calculated as:

$$f(m) = |\mathcal{A}|^2 / \int |\mathcal{A}|^2 dm , \quad (2.33)$$

where the amplitude is, as often done in the literature, parametrized in the form:

$$\mathcal{A} = \mathcal{A}_{BW} \frac{\sqrt{m m_\rho} \Gamma(m)}{m^2 - m_\rho^2 + i m_\rho \Gamma(m)} + \mathcal{A}_{\pi\pi} . \quad (2.34)$$

The mass-dependent width is parametrized as in [8]

$$\Gamma(m) = \Gamma_\rho \frac{m_\rho}{m} \left(\frac{m^2 - 4m_\rho^2}{m_\rho^2 - 4m_\pi^2} \right)^{3/2} , \quad (2.35)$$

i.e. vanishes below the two-pion threshold and as a consequence also the spectral shape vanishes below the two-pion threshold. The extra constant is often added to describe a big asymmetry (enhancement of the left hand side of the ρ^0 resonance). A physical interpretation of the constant term for proton-proton collisions can be found in Ref. [20] where it was described as due to the Deck two-pion continuum.

In the following we shall parametrize the first term in Eq. (2.21) for the resonance mass ($m_\rho = 770$ MeV) (see [5]). However, we shall include the running masses (m_1 and m_2) in calculating t_{max} . This leads to a deformation of the spectral shapes of resonances. One could also include the dependence of the production cross section on running masses which would lead to an extra deformation. These deformations have an influence on the actual value of the integrated cross section, which will be discussed in the next section.

In Fig. 4 we show the invariant-mass distribution of single ρ^0 production. The ρ^0 peak is asymmetric. Clearly the left hand flank is enhanced due to production mechanism discussed in the previous section. This asymmetry is opposite than in many other processes.

In Fig. 5 we show two-dimensional distributions in masses of both ρ^0 mesons for double- ρ^0 production. A strong enhancement at low masses is again clearly visible. The enhancement of the low masses may lead to an enhancement of the cross section compared to fixed-mass calculation. This will be discussed in the section III where our results will be presented.

E. $\rho^0 \rightarrow \pi^+ \pi^-$ decays

The ρ^0 mesons from photoproduction are dominantly transversely polarized and have negligibly small transverse momenta with respect to the direction of heavy ions. We parametrize

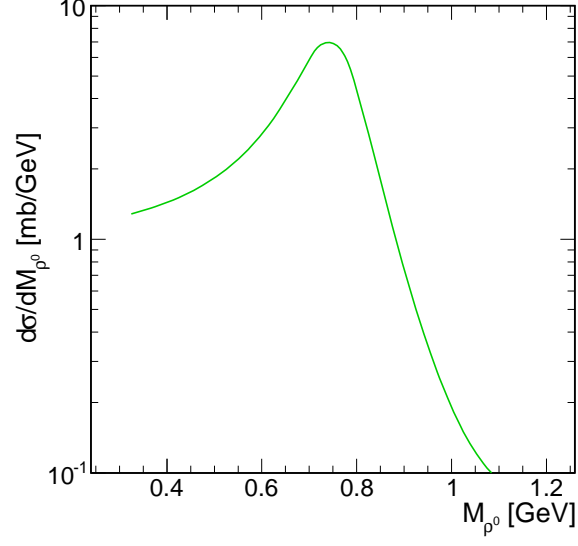


FIG. 4: Distribution in the mass of one of ρ^0 meson produced in double scattering mechanism. An enhancement at lower M_{ρ^0} is clearly visible.

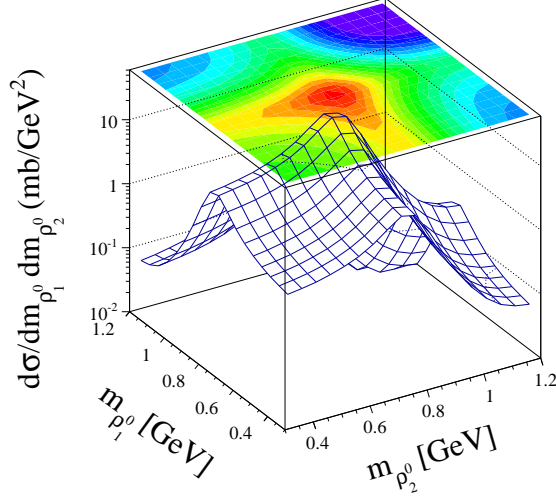


FIG. 5: Two-dimensional distribution in ρ^0 meson masses produced in the double scattering mechanism. An enhancement at lower m_1 and m_2 is clearly visible.

the decay function in the ρ^0 center of mass as:

$$f(\theta^*) = \frac{3}{2} \sin^2(\theta^*) . \quad (2.36)$$

The calculations are done as follows. First a map of the cross section for a dense grid in (y_1, y_2) is prepared in the case of double scattering with fixed ρ^0 meson masses (the corresponding ρ^0 mesons have negligibly small transverse momenta) or in (y_1, y_2, m_1, m_2) when the smearing of the ρ^0 mass is taken into account. For the $\gamma\gamma$ mechanism one has to

take into account in addition the transverse momenta of the ρ^0 mesons as dictated by the VDM-Regge or two-gluon exchange models.

Then the decays are done in a separate Monte Carlo code. The distributions in ρ^0 centers of mass are generated randomly with the decay function given by (2.36) or isotropically. Next a Lorentz transformations to the overall ion-ion center of mass (laboratory system for both RHIC and LHC) is performed. Different kinematical variables related to charged pions are calculated and corresponding distributions are obtained by an appropriate binning. Since we have the full kinematics of the event any cut on kinematical variables can be easily imposed.

III. FIRST NUMERICAL RESULTS

Having fixed the details of single vector meson production we can now proceed to the production of two vector mesons. For the RHIC energy we consider $^{197}\text{Au} + ^{197}\text{Au}$ collisions and for the LHC energy we take into account $^{208}\text{Pb} + ^{208}\text{Pb}$ collisions. As an example in Table I we show total cross section for $\rho^0\rho^0$ production in ultraperipheral, ultrarelativistic heavy ion collisions. The double scattering cross section for $\rho^0\rho^0$ pair production at RHIC energy is about 1.5 mb. This is a rather large cross section (compared to the cross section for exclusive production of $\rho^0\rho^0$ via photon-photon fusion which at RHIC energy $\sqrt{s_{NN}} = 200$ GeV is of the order of 0.1 mb)². More details can be found in our previous paper [2] and in Table I. The cross section for the smeared ρ^0 masses is larger than that for larger than that for fixed resonance masses. The cross section for the VDM-Regge contribution is rather small. Its relative contribution should increase at LHC energies where the photon-photon luminosities are much larger.

TABLE I: Cross sections (in mb) for single ρ^0 production and double scattering and photon-photon mechanisms of $\rho^0\rho^0$ production for fixed and smeared mass of ρ^0 meson.

Energy	$m_{\rho^0} = 0.77549 \text{ GeV}$	Mass smearing
RHIC ($\sqrt{s_{NN}} = 200 \text{ GeV}$), single ρ^0 production	596	
LHC ($\sqrt{s_{NN}} = 3.5 \text{ TeV}$), single ρ^0 production	4000	
LHC ($\sqrt{s_{NN}} = 5.5 \text{ TeV}$), single ρ^0 production	4795	
RHIC ($\sqrt{s_{NN}} = 200 \text{ GeV}$), double scattering	1.5	1.55
LHC ($\sqrt{s_{NN}} = 3.5 \text{ TeV}$), double scattering		15.25
RHIC ($\sqrt{s_{NN}} = 200 \text{ GeV}$), double scattering, $ \eta_\pi < 1$		0.15
LHC ($\sqrt{s_{NN}} = 3.5 \text{ TeV}$), double scattering, $ \eta_\pi < 1$		0.3
RHIC ($\sqrt{s_{NN}} = 200 \text{ GeV}$), $\gamma\gamma$, VDM-Regge	$7.5 \cdot 10^{-3}$	
RHIC ($\sqrt{s_{NN}} = 200 \text{ GeV}$), $\gamma\gamma$, low-energy bump	$95 \cdot 10^{-3}$	
RHIC ($\sqrt{s_{NN}} = 200 \text{ GeV}$), $\gamma\gamma$, VDM-Regge, $ \eta_\pi < 1$	$0.5 \cdot 10^{-3}$	
RHIC ($\sqrt{s_{NN}} = 200 \text{ GeV}$), $\gamma\gamma$, low-energy bump, $ \eta_\pi < 1$	$14.6 \cdot 10^{-3}$	

² For comparison the cross section for $PbPb \rightarrow PbPb\pi^+\pi^-$ via photon-photon fusion at $\sqrt{s_{NN}} = 3.5 \text{ TeV}$ is 46.7 mb [21].

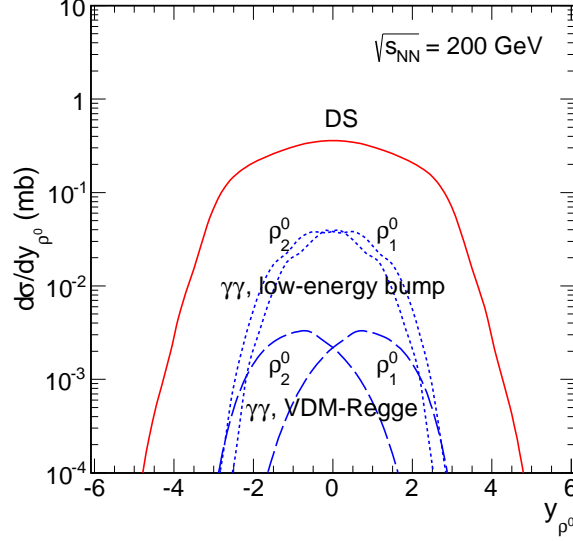


FIG. 6: Rapidity distribution of one of ρ^0 mesons produced in double scattering mechanism. The double-scattering contribution is shown by the solid (red online) line and the dashed lines (blue online) represents distributions of forward and backward ρ^0 produced in the VDM-Regge photon-photon fusion.

Distributions in ρ^0 meson rapidity is shown in Fig. 6. One can observe a clear dominance of the double scattering component over the photon-photon component. At the LHC the proportions should be slightly different. For the photon-photon mechanism we show separate contributions for the forward and backward ρ^0 mesons.

Now we wish to discuss briefly the contributions of individual diagrams of Fig. 3 to (y_1, y_2) two dimensional distribution. The corresponding distributions are shown in Fig. 7. The distributions for different combinations are identical in shape but located in different corners in (y_1, y_2) space.

A full (including all contributions) two-dimensional distribution in rapidity of each of the mesons is shown in Fig. 8 which in the approximations made is a sum of the individual contributions. The distribution is rather flat in the entire (y_1, y_2) space (see the left panel). This is in contrast to the two-photon processes, where the cross section is concentrated along the $y_1 = y_2$ diagonal (see the right panel). In principle, this clear difference can be used to distinguish the double photoproduction from the photon-photon fusion. The asymmetry with respect to $y_1 = y_2$ line for the photon-photon mechanism is due to our convention where y_1 denotes rapidity of the forward and y_2 rapidity of the backward emitted ρ^0 mesons. This can be done only in model calculation.

The corresponding distribution in the $\rho^0\rho^0$ invariant mass is shown in Fig. 9. In general, somewhat larger invariant masses are generated via the double scattering mechanism than in two-photon processes. The reader is asked to compare the present plot with analogous plot in Ref. [2].

In real experiments, charged pions are measured rather than ρ^0 mesons. Therefore, we now proceed to a presentation of some observables related to charged pions. We start from the presentation of four-pion invariant mass distribution (see Fig. 10). The distribution for the whole phase space extends to large invariant masses, while the distribution in the

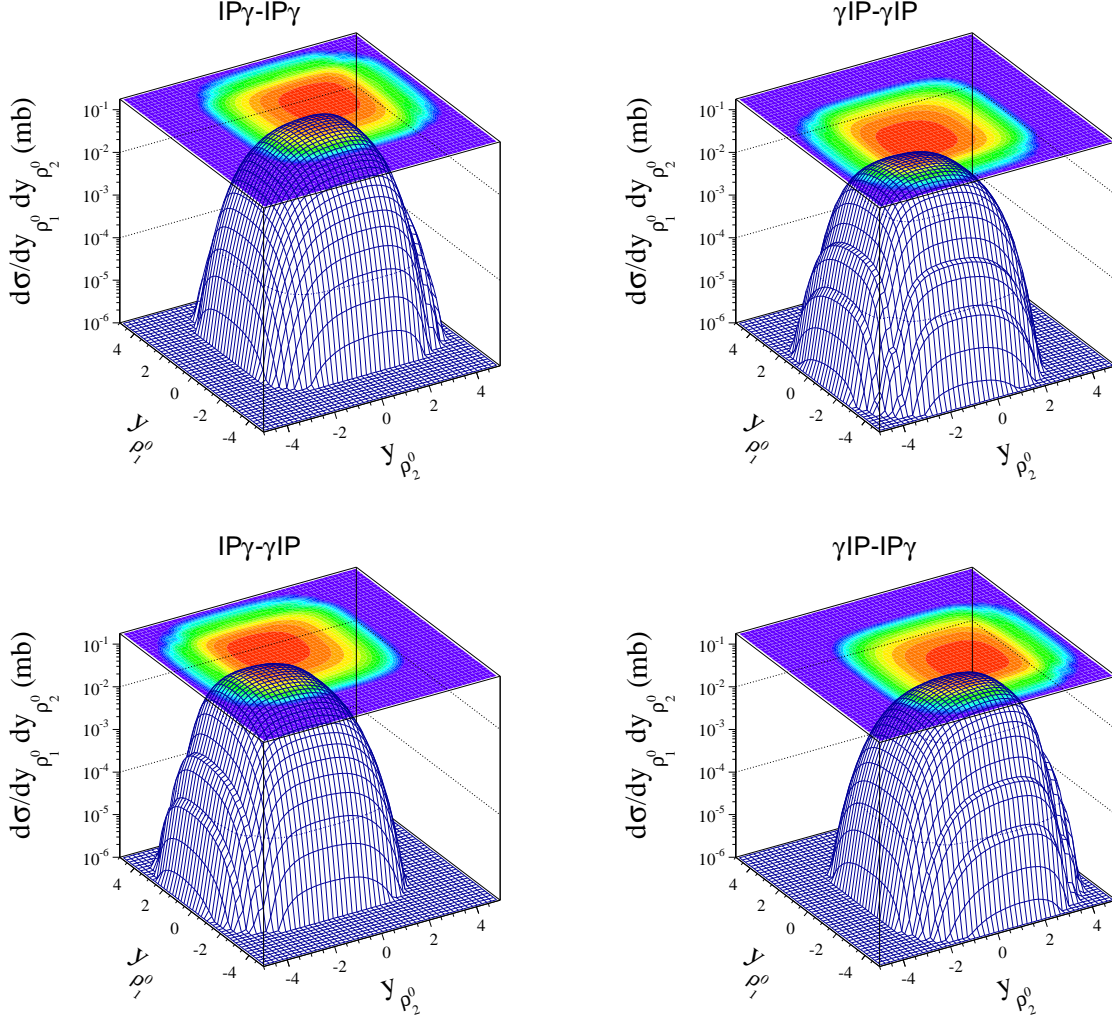


FIG. 7: Contributions of individual diagrams of Fig. 3 to two-dimensional distribution in ρ^0 meson rapidities for double scattering production for the full phase space at $\sqrt{s_{NN}} = 200$ GeV.

limited range of (pseudo)rapidity spanned by the STAR detector give a shape similar to the measured distribution (see dash-dotted line in the right panel of Fig. 10). However, the double-scattering contribution accounts only for 20 % of the cross section measured by the STAR collaboration [22]. Apparently, the production of the $\rho^0(1700)$ resonance and its subsequent decay into the four-pion final state (see e.g., [24]) is the dominant effect for the limited STAR acceptance. Both, the production mechanism of $\rho^0(1700)$, and its decay into four charged pions are not yet understood. We therefore leave the modeling of these production and decay processes for a separate study.

In Fig. 11 we show distributions in pseudorapidity of the charged pions. The distributions extend over a broad range of pseudorapidity. Both STAR collaboration at RHIC and the ALICE collaboration at LHC can observe only a small fraction of pions due to the rather limited angular (pseudorapidity) coverage $\eta \sim 0$. While the CMS (pseudo)rapidity coverage is wider, it is not clear to us if the CMS collaboration has a relevant trigger to measure the exclusive nuclear processes described here.

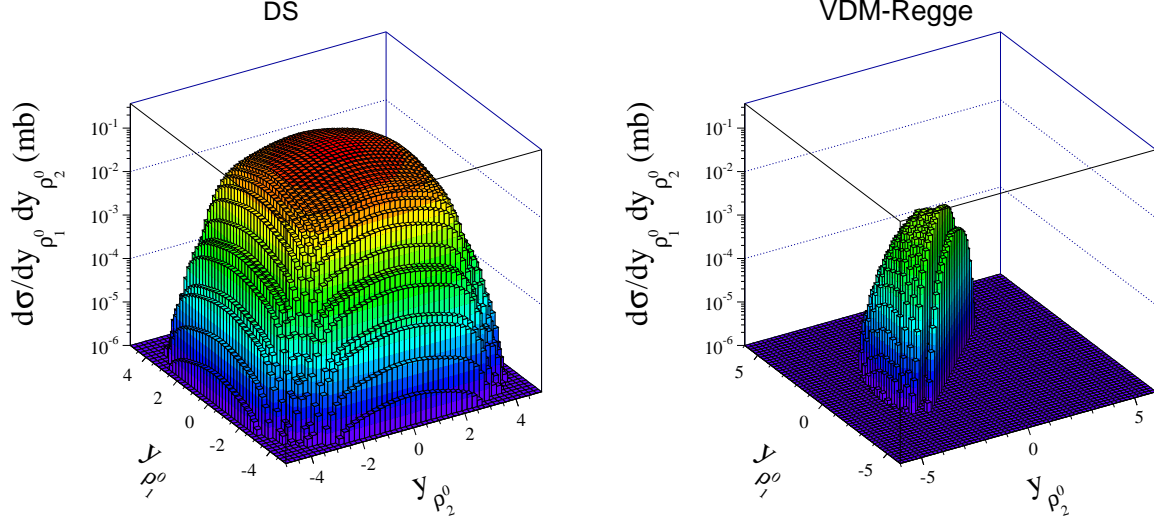


FIG. 8: Two-dimensional distribution (y_1, y_2) in ρ^0 meson rapidities for double scattering (left panel) and VDM-Regge photon-photon (right panel) production for the full phase space at $\sqrt{s_{NN}} = 200$ GeV. The distribution for $\gamma\gamma$ subprocess is asymmetric because in this case the first ρ^0 is emitted in forward direction and the second ρ^0 is emitted in backward direction.

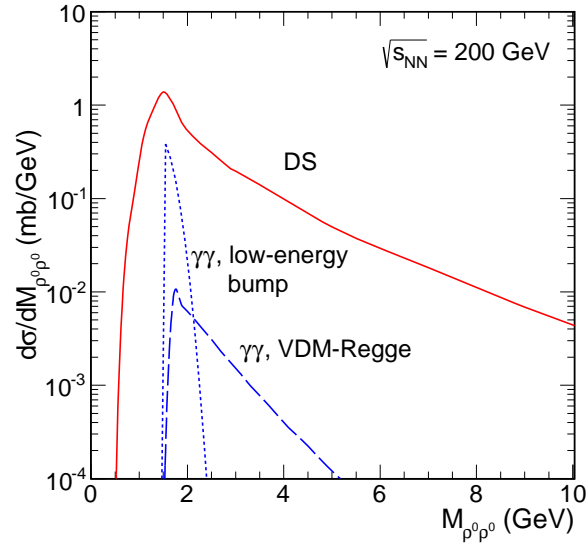


FIG. 9: Invariant mass distribution of $\rho^0\rho^0$ for double scattering (solid line), VDM-Regge photon-photon (dashed line) and low-energy bump (dotted line) mechanisms for full phase space at $\sqrt{s_{NN}} = 200$ GeV.

For completeness in Fig. 12 we show distributions in pion transverse momenta. Since the ρ^0 mesons produced in the double-scattering mechanism (photon-pomeron or pomeron-photon fusion) have very small transverse momenta, the transverse momenta of pions are limited to $\sim m_{\rho^0}/2$. The distribution is relatively smooth, as we have taken into account a smearing of ρ^0 meson masses. The sharp upper limit is an artifact of our maximal value of ρ^0

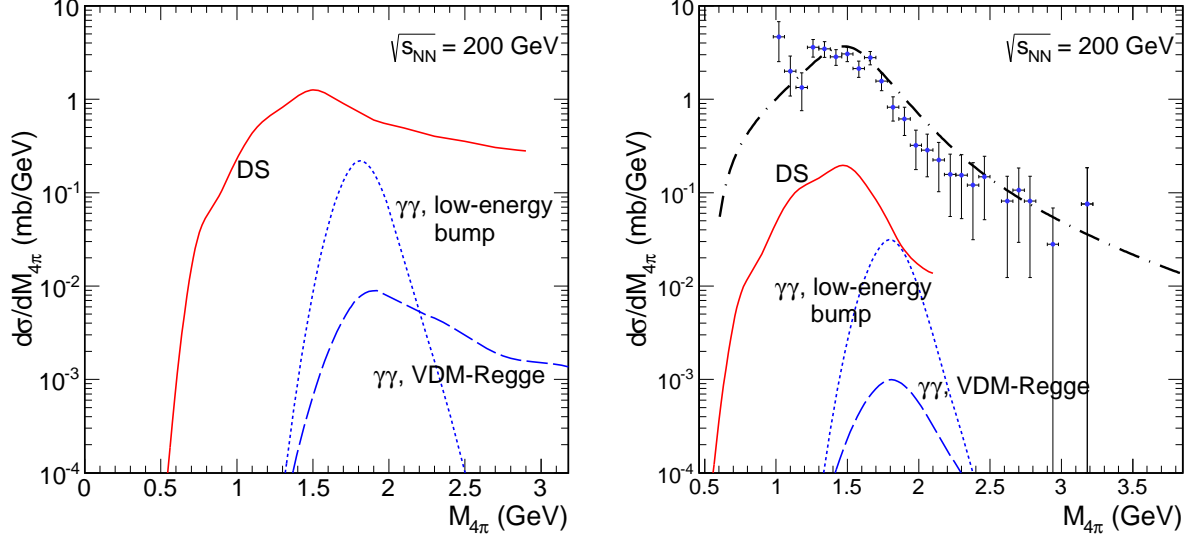


FIG. 10: Four-pion invariant mass distribution for double scattering mechanism (solid line), VDM-Regge photon-photon (dashed line) and low-energy bump (dotted line) mechanisms for full phase space (left panel) and for the limited acceptance STAR experiment (right panel) at $\sqrt{s_{NN}} = 200$ GeV. The STAR experimental data [22] have been corrected by acceptance function [23]. The dash-dotted line represents a fit of the STAR collaboration.

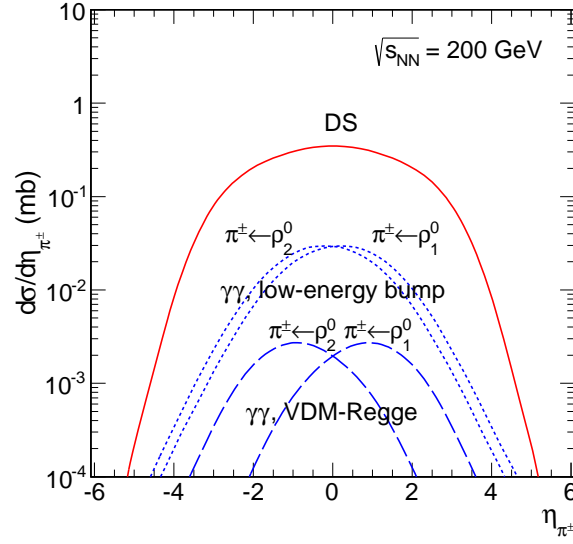


FIG. 11: Pseudorapidity distribution of charged pions for double scattering (solid line), VDM-Regge photon-photon (dashed line) and low-energy bump (dotted line) mechanisms for full phase space at $\sqrt{s_{NN}} = 200$ GeV.

meson mass $m_\rho^{max} = 1.2$ GeV. We have imposed this upper limit because the spectral shape of “ ρ^0 meson” above $m_\rho > 1.2$ GeV is not under good theoretical control. In principle, at larger $p_{t,\pi}$, the contribution coming from the decay of ρ^0 meson produced in photon-photon

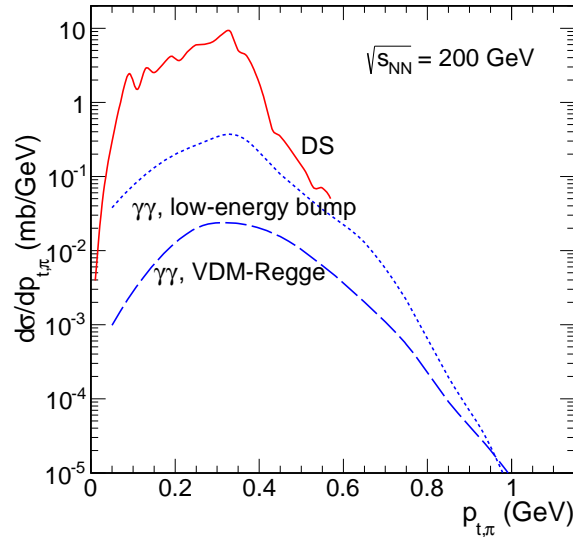


FIG. 12: Transverse momentum distribution of charged pions for double scattering (solid line) low-energy bump (dotted line) and VDM-Regge photon-photon (dashed line) mechanisms for full phase space at $\sqrt{s_{NN}} = 200$ GeV.

fusion can be larger as that of double scattering mechanism, as the transverse momentum of ρ^0 mesons are not strictly limited to small values. However, the cross section for such cases is expected to be rather small. Both STAR ($p_t > 0.1$ GeV) and ALICE ($p_t > 0.1$ GeV) experiments have a fairly good coverage in pion transverse momenta and could measure such distributions.

IV. CONCLUSIONS

In this work we have studied two- ρ^0 as well as four-pion production in exclusive ultraperipheral heavy ion collisions, concentrating on the double scattering mechanism of single ρ^0 production.

Differential distributions for the two ρ^0 mesons, as well as for four pions have been presented. The results (total cross section and differential distributions) for the double scattering mechanism have been compared with the results for two-photon fusion discussed previously in the literature. We have found that at the RHIC energy $\sqrt{s_{NN}} = 200$ GeV the contribution of double scattering is almost two orders of magnitude larger than that for the photon-photon mechanism.

The produced ρ^0 mesons decay, with almost 100 % probability, into charged pions giving large contribution to exclusive production of the $\pi^+\pi^-\pi^+\pi^-$ final state. We have made a comparison of four pion production via $\rho^0\rho^0$ production (double scattering and photon-photon fusion) with experimental data measured by the STAR collaboration for the $AuAu \rightarrow AuAu\pi^+\pi^-\pi^+\pi^-$ reaction. The theoretical predictions have a similar shape in four-pion invariant mass as measured by the STAR collaboration (in a limited interval of pion pseudorapidity and transverse momenta), but exhaust only about 20 % of the measured cross section. The missing contribution is probably due to the exclusive production

of $\rho^0(1700)$ (excited state of $\rho^0(770)$) resonance and its decay into four charged pions. We leave a theoretical calculation for the latter mechanism for a separate analysis. We expect that in the total phase space the contribution of double scattering is similar to that for the $\rho^0(1700)$ resonant production.

At large $\rho^0\rho^0$ (pseudo)rapidity separations and/or large $\pi^+\pi^+$ ($\pi^-\pi^-$) (pseudo)rapidity separations the double scattering contribution should dominate over other contributions. The identification of the dominance region seems difficult, if not impossible, at RHIC.

The four charged pion final state is being analyzed by the ALICE collaboration. We plan a separate careful analysis for the ALICE and/or other LHC experiments. It would be interesting if different mechanisms discussed in the present paper could be separated and identified experimentally in the future. This requires, however, rather complicated correlation studies for four charged pions. Such a study will be presented elsewhere.

Similar double scattering mechanisms could be studied for different vector meson production, e.g., for exclusive production of $\rho^0 J/\Psi$. Recently we have studied production of $J/\Psi J/\Psi$ pairs via two-photon mechanism in exclusive heavy ion reactions [12]. A calculation of the corresponding double-scattering contribution is very interesting in the present context.

Acknowledgments

We are indebted to Boris Grube for a discussion of the STAR experimental data and explanation of some details as well as providing us numerical representation of the STAR experimental data. The discussion with Daniel Tapia Takaki about four pion production at ALICE (LHC) is kindly acknowledged. The careful reading of the manuscript by Christoph Mayer is acknowledged. This work was partially supported by N N202 236640 and N DEC-2011/01/B/ST2/04535. A big part of the calculations within this analysis was carried out with the help of the cloud computer system (Cracow Cloud One ³) of Institute of Nuclear Physics (PAN).

-
- [1] V.M. Budnev, I.F. Ginzburg, G.V. Meledin and V.G. Serbo, Phys. Rep. **15** (1975) 4; C.A. Bertulani and G. Baur, Phys. Rep. **163** (1988) 29; G. Baur, K. Hencken, D. Trautmann, S. Sadovsky, and Y. Kharlov, Phys. Rep. **364** (2002) 359; C.A. Bertulani, S.R. Klein and J. Nystrand, Ann. Rev. Nucl. Part. Sci. **55** (2005) 271; A.J. Baltz, G. Baur, D. d'Enterria et al., Phys. Rep. **458** (2008) 1.
 - [2] M. Khusek, W. Schäfer and A. Szczurek, Phys. Lett. **B674** (2009) 92.
 - [3] V.P. Goncalves and M.V.T. Machado, Eur. Phys. J. **C29** (2003) 271.
 - [4] V.P. Goncalves, M.V.T. Machado and W.K. Sauter, Eur. Phys. J. **C46** (2006) 219.
 - [5] S.R. Klein and J. Nystrand, Phys. Rev. **C60** (1999) 014903.
 - [6] L. Frankfurt, M. Strikman and M. Zhalov, Phys. Rev. **C67** (2003) 034901.
 - [7] V.P. Goncalves and M.V.T. Machado, Eur. Phys. J. **C40** (2005) 519.
 - [8] STAR Collaboration, B.I. Abelev et al., Phys. Rev. **C77** (2008) 034910.
 - [9] LHCb Collaboration, R. Aaij et al., J. High Energy Phys. **06** (2012) 141.
 - [10] M. Luszczak, R. Maciula and A. Szczurek, Phys. Rev. **D84** (2011) 114018; R. Maciula and A. Szczurek, Phys. Rev. **D87** (2013) 074039.

³ cc1.ifj.edu.pl

- [11] TASSO Collaboration, M. Althoff et al., Z. Phys. **C16** (1982) 13; CELLO Collaboration, H.J. Behrend et al., Z. Phys. **C21** (1984) 205; TWO-GAMMA Collaboration, H. Aihara et al., Phys. Rev. **D37** (1988) 28; PLUTO Collaboration, Ch. Berger et al., Z. Phys. **C38** (1988) 521; ARGUS Collaboration, H. Albrecht et al., Z. Phys. **C50** (1991) 1; L3 Collaboration, P. Achard et al., Phys. Lett. **B568** (2003) 11.
- [12] S. Baranov, A. Cisek, M. Khusek-Gawenda, W. Schäfer and A. Szczurek, Eur. Phys. Jour. **C73** (2013) 2335.
- [13] A. Donnachie and P.V. Landshoff, Phys. Lett. **B296** (1992) 227.
- [14] V.P. Goncalves and M.V.T. Machado, J. Phys. G. **32** (2006) 295.
- [15] T. Lappi and H. Mäntysaari, Phys. Rev. **C87** (2013) 032201.
- [16] A. Cisek, W. Schäfer and A. Szczurek, Phys. Rev. **C86** (2012) 014905.
- [17] B.Z. Kopeliovich, J. Nemchik, N.N. Nikolaev and B.G. Zakharov, Phys. Lett. **B309** (1993) 179; Phys. Lett. **B324** (1994) 469.
- [18] J. Nemchik, N.N. Nikolaev and B.G. Zakharov, Phys. Lett. **B341** (1994) 228); J. Nemchik, N.N. Nikolaev, E. Predazzi and B.G. Zakharov, Z. Phys. **C75** (1997) 71.
- [19] N.N. Nikolaev and B.G. Zakharov, Z. Phys. **C49** (1991) 607.
- [20] A. Szczurek and A.P. Szczepaniak, Phys. Rev. **D71** (2005) 054005.
- [21] M. Khusek-Gawenda and A. Szczurek, Phys. Rev. **C87** (2013) 054908.
- [22] STAR Collaboration, B.I. Abelev et al., Phys. Rev. **C81** (2010) 044901.
- [23] Boris Grube, private communication.
- [24] J. Beringer et al. (Particle Data Group), Phys. Rev. **D86** (2012) 010001.